JACS
JOURNAL OF THE AMERICAN CHEMICAL SOCIETY

Article

pubs.acs.org/JACS

Ultrasensitive Near-Infrared Fluorescence-Enhanced Probe for *in Vivo* Nitroreductase Imaging

Yuhao Li, Yun Sun, Jiachang Li, Qianqian Su, Wei Yuan, Yu Dai, Chunmiao Han, Qiuhong Wang, Wei Feng,* and Fuyou Li*

Department of Chemistry and State Key Laboratory of Molecular Engineering of Polymers and Collaborative Innovation Center of Chemistry for Energy Materials, Fudan University, Shanghai 200433, P. R. China

Supporting Information

ABSTRACT: Nitroreductase (NTR) can be overexpressed in hypoxic tumors, thus the selective and efficient detection of NTR is of great importance. To date, although a few optical methods have been reported for the detection of NTR in solution, an effective optical probe for NTR monitoring *in vivo* is still lacking. Therefore, it is necessary to develop a near-infrared (NIR) fluorescent detection probe for NTR. In this study, five NIR cyanine dyes with fluorescence reporting structure decorated with different nitro aromatic groups, Cy7-1−5, have been designed and explored for possible rapid detection of NTR. Our experimental results presented that only a *para*-nitro benzoate group modified cyanine probe (Cy7-1) could serve as a rapid NIR fluorescence-enhanced probe for monitoring and bioimaging of NTR. The structure−function relationship has been revealed by theoretical study. The linker connecting the detecting and fluorescence reporting groups and the nitro group position is a key factor for the formation of hydrogen bonds and spatial structure match, inducing the NTR catalytic ability enhancement. The *in vitro* response and mechanism of the enzyme-catalyzed reduction of Cy7-1 have been investigated through kinetic optical studies and other methods. The results have indicated that an electro-withdrawing group induced electron-transfer process becomes blocked when Cy7-1 is catalytically reduced to Cy7-NH_2 by NTR, which is manifested in enhanced fluorescence intensity during the detection process. Confocal fluorescence imaging of hypoxic A549 cells has confirmed the NTR detection ability of Cy7-1 at the cellular level. Importantly, Cy7-1 can detect tumor hypoxia in a murine hypoxic tumor model, showing a rapid and significant enhancement of its NIR fluorescence characteristics suitable for fluorescence bioimaging. This method may potentially be used for tumor hypoxia diagnosis.

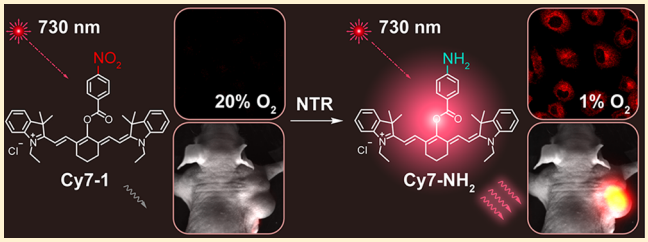

INTRODUCTION

Hypoxia is a feature of tumor tissue, whereby the median oxygen (O_2) concentration in some solid tumors is ∼4% and may even decrease to 0% locally.[1] In clinical application, the formation of hypoxic tumors with abnormal microvessels can limit the perfusion of cytotoxic chemotherapeutic drugs therein, decreasing their curative effect compared with that in normoxic tumors. Therefore, estimating the tumor hypoxia degree is of great importance in predicting anticancer efficacies. To date, several methods have been developed to evaluate the tumor hypoxia degree, such as oxygen pressure measurement methods (e.g., the oxygen electrode method), blood flow velocity methods (e.g., blood oxygenation level dependent magnetic resonance imaging (BLOD-MRI)), hypoxia marker detection methods (e.g., nitroreductase, hypoxia inducible factor (HIF)), and so on.[1]

Because of its high selectivity and sensitivity, biomarker detection represents a very important detection method for hypoxia. Generally, hypoxia is accompanied by elevated levels of reductive enzymes such as nitroreductase (NTR), DT-diaphorase, and azoreductase. In the solid tumor, the NTR level is directly related to the degree of hypoxia. Thus, the detection of the NTR level can be used to evaluate the hypoxic degree of a tumor.[2]

According to the previously reported NTR-catalyzed reactions, aromatic substrates show relatively high reactivity with NTR due to strong interaction between the two caused by hydrogen bonding, $\pi-\pi$ stacking interaction, hydrophobic effect, and etc. The nitro groups in substrates can be reduced first to a nitroso group, then a hydroxylamine group, and ultimately to an amino group.[3] In addition, the electron-withdrawing group induces an electron-transfer process, quenching the fluorescence emission of a substrate, and the reduction of nitro groups by NTR leads to a change in fluorescence intensity. These fundamental considerations underpin an important strategy in the design of fluorescent probes for NTR detection.[4] Qian's group, Ma's group, and other groups reported several fluorescent probes by connecting aromatic nitro groups to visible-excited fluorophores (such as naphthalimide, nile blue, and resorufin).[5−7] However, these probes required ultraviolet (UV) or visible light as the

Received: April 20, 2015
Published: April 29, 2015

DOI: 10.1021/jacs.5b04097
J. Am. Chem. Soc. 2015, 137, 6407−6416

excitation source, causing a possible detrimental effect on healthy cells and organs.[8,9] Recently, Tang's group reported a cyanine derivative as a near-infrared (NIR) fluorescent turn-on probe (λ_{ex} = 690 nm, λ_{em} = 750 nm) to detect NTR.[10] Unfortunately, no *in vivo* animal bioimaging was carried out. This may have been because this NIR probe showed a limited fluorescence enhancement (four-fold). Therefore, the development of an effective probe allowing optical detection of NTR for *in vivo* imaging, characterized by fast response, ultrasensitivity, and an NIR optical window with excitation and emission wavelengths >700 nm, still remains a significant challenge.

Inspired by the structure and spatial arrangement of enzyme, we reasoned that the design principle involves not only the interaction between NTR and substance, the substituent group of substance, but also the structural and spatial match−mismatch of these two. Herein, we designed and synthesized five cyanine probes decorated with the nitro aromatic groups (Cy7-1−5, Scheme 1) for detection of NTR. Our mechanistic

Scheme 1. Chemical Structures of Five Fluorescent Probes Cy7-1−5

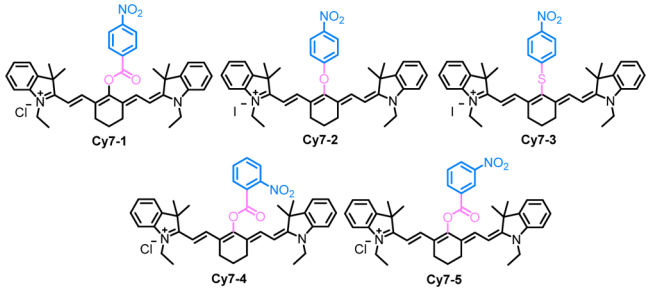

investigation and docking theoretical calculations show that the spatial structure of a probe and hydrogen-bonding interaction between the probe and NTR are the critical points, which have been significantly influenced by the probes' linker and nitro substituent position, inducing the change of NTR detection ability. Importantly, a remarkable NIR fluorescent OFF−ON probe Cy7-1 for NTR detection is developed and systematically studied. Cy7-1 qualifies NIR excitation and shows emission at >750 nm (λ_{ex} = 769 nm, λ_{em} = 788 nm), an ideal profile for penetration through thicker biological specimens, and exhibits a rapid, selective, and sensitive fluorescence turn-on response to NTR with a 110-fold enhancement. Furthermore, we established the ability of Cy7-1 to monitor overexpressed nitroreductase in hypoxic cells *in vitro*. Finally, we applied Cy7-1 for monitoring intratumoral NTR by an *in vivo* fluorescence bioimaging technique, highlighting the potential diagnostic value of this NIR probe.

EXPERIMENTAL SECTION

Chemicals and Instruments. All chemicals were purchased from J&K Scientific Ltd. or Sinopharm chemical reagent Co. Ltd. and were used without any further purification. The silica gel (100−200 mesh) was used for the flash chromatography. Nitroreductase from *Escherichia coli* was purchased from Sigma-Aldrich Co. Ltd. β-Nicotinamide adenine dinucleotide disodium salt hydrate (NADH) was purchased from TCI Co. Ltd. Ultrapure water was collected from a Milli-Q reference system. The ^{18}F-FMISO (3-fluoro-1-(2′-nitro-1′-imidazolyl)-2-propanol) in 0.9% NaCl aqueous solution was supplied by Fudan University Shanghai Cancer Center.

The compounds were characterized by ^{1}H NMR, ^{13}C NMR, or (and) MALDI-Tof/Tof mass spectra (MALDI-Tof/Tof-MS). ^{1}H NMR and ^{13}C NMR spectra were obtained on a Bruker 400 MHz NMR spectrometer, tetramethylsilane (TMS) as internal standard (0 ppm) substances, and MeOD or $CDCl_3$ as solvent. MALDI-Tof/Tof-MS spectra were measured on an AB SCIEX 5800 matrix-assisted laser desorption ionization time-of-flight/time-of-flight mass spectrometer. A Shimadzu UV-2550 UV−vis-NIR spectrometer was used to measure the UV−vis absorption spectra, and an Edinburgh LFS-920 fluorescence spectrometer with 450 W xenon lamp or Edinburgh FS5 fluorescence spectrometer with 150 W xenon lamp was utilized to obtain the steady-state emission spectra. The absolute emission quantum yields were monitored by Hamamatsu Quantaurus-QY system.

Synthesis of Compound Cy7-OH. Compound Cy7-OH was synthesized according to the literature reported method[11] with some modifications, as shown in Scheme 2. Compound Cy7-Cl (480 mg,

Scheme 2. Synthetic Routine of the Probe Cy7-1

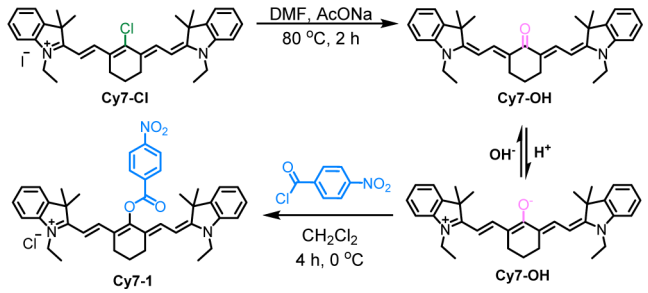

0.751 mmol, 1 equiv) and sodium acetate (185 mg, 2.25 mmol, 3 equiv) were dissolved in anhydrous *N*,*N*-dimethylformamide (20 mL), and the solution was heated at 80 °C for 2 h under argon protection. The solvent was then removed under reduced pressure. The crude product was purified by chromatography on silica (SiO_2; CH_2Cl_2/CH_3OH, 100:1, v/v) to afford a red solid, 304 mg, 65% yield. ^{1}H NMR (400 MHz, $CDCl_3$) δ 8.18 (d, J = 13.1 Hz, 1H), 7.18 (d, J = 6.6 Hz, 2H), 6.91 (t, J = 7.4 Hz, 1H), 6.68 (d, J = 8.0 Hz, 1H), 5.47 (d, J = 13.2 Hz, 1H), 3.74 (q, J = 7.0 Hz, 2H), 2.62 (t, J = 5.6 Hz, 2H), 1.92−1.81 (m, 1H), 1.67 (s, 6H), 1.27 (t, J = 7.1 Hz, 3H). ^{13}C NMR (101 MHz, $CDCl_3$) δ 143.71, 139.83, 132.83, 127.63, 121.81, 120.45, 106.39, 92.14, 46.58, 37.04, 28.69, 25.84, 22.55, 11.14. MALDI-Tof/Tof-MS calcd for $C_{34}H_{40}N_2O$ 492.3141, found 492.3124 (Scheme S1, Figures S1−S5).

General Synthetic Procedure for Compounds Cy7-1, Cy7-4, and Cy7-5. Compound Cy7-OH (494.7 mg, 0.404 mmol, 1 equiv) was dissolved in dry CH_2Cl_2 (15 mL), and the solution was cooled to 0 °C. A solution of nitrobenzoyl chloride (188 mg, 1.011 mmol, 2.5 equiv) in CH_2Cl_2 (5 mL) was then added dropwise within 10 min under argon protection. The mixture was allowed to react for a further 20 min at 0 °C, then the ice bath was removed, and the mixture was allowed to warm to room temperature over a period of 3.5 h. The reaction was monitored by thin layer chromatography (TLC). After its completion, the solvent was removed, and the crude product was purified by flash column chromatography (SiO_2; CH_2Cl_2/CH_3OH, 20:1, v/v) to afford the target compound (Schemes 2, S2, and Figures S6−S14).

Cy7-1. A green solid with a metallic luster, 210 mg, 77% yield. ^{1}H NMR (400 MHz, MeOD) δ 8.61 (dd, J = 23.4, 9.0 Hz, 4H), 7.81 (d, J = 14.2 Hz, 2H), 7.44−7.34 (m, 4H), 7.28 (d, J = 7.9 Hz, 2H), 7.21 (t, J = 7.4 Hz, 2H), 6.25 (d, J = 14.1 Hz, 2H), 4.18 (q, J = 7.2 Hz, 4H), 3.35 (s, 1H), 2.78 (s, 4H), 2.13−1.98 (m, 2H), 1.37 (t, J = 7.2 Hz, 17H). ^{13}C NMR (101 MHz, MeOD) δ 171.83, 162.55, 159.25, 151.86, 141.64, 141.08, 140.08, 133.18, 131.38, 128.49, 125.06, 124.35, 122.10, 121.10, 110.54, 99.95, 48.95, 38.87, 26.69, 23.89, 20.76, 11.04. MALDI-Tof/Tof-MS calcd for $C_{41}H_{44}N_3O_4^+$ 642.3326 $[M]^+$, found 642.3356 $[M]^+$.

DOI: 10.1021/jacs.5b04097
J. Am. Chem. Soc. 2015, 137, 6407−6416

Cy7-4. A green solid with a metallic luster, 130 mg, 48% yield. ^{1}H NMR (400 MHz, MeOD) δ 8.44 (d, J = 7.2 Hz, 1H), 8.01 (dddd, J = 36.7, 30.9, 18.0, 4.9 Hz, 4H), 7.79 (d, J = 14.0 Hz, 2H), 7.65 (t, J = 6.4 Hz, 1H), 7.41 (dt, J = 7.0, 3.6 Hz, 4H), 7.34−7.21 (m, 4H), 6.25 (d, J = 14.1 Hz, 2H), 4.21 (q, J = 7.1 Hz, 4H), 2.80−2.71 (m, 4H), 1.42 (dd, J = 24.7, 17.5 Hz, 18H). ^{13}C NMR (101 MHz, MeOD) δ 171.89, 161.18, 141.64, 141.33, 140.03, 140.02, 135.51, 132.65, 132.46, 132.16, 128.91, 128.54, 128.45, 125.06, 124.15, 123.12, 122.03, 121.45, 121.29, 110.55, 100.18, 61.34, 49.01, 38.84, 38.83, 26.53, 24.04, 20.70, 11.02, 11.00. MALDI-Tof/Tof-MS calcd for $C_{41}H_{44}N_3O_4^+$ 642.3326 $[M]^+$, found 642.1550 $[M]^+$.

Cy7-5. A green solid with a metallic luster, 150 mg, 55% yield. ^{1}H NMR (400 MHz, MeOD) δ 9.20−9.13 (m, 1H), 8.78 (t, J = 8.1 Hz, 2H), 8.06 (t, J = 8.0 Hz, 1H), 7.84 (d, J = 14.1 Hz, 2H), 7.32 (tt, J = 33.2, 7.8 Hz, 10H), 6.27 (d, J = 14.2 Hz, 2H), 4.20 (dd, J = 14.5, 7.2 Hz, 4H), 2.80 (s, 4H), 1.48−1.27 (m, 18H). ^{13}C NMR (101 MHz, MeOD) δ 171.83, 171.81, 162.34, 148.98, 141.64, 141.08, 140.08, 140.07, 135.52, 131.27, 131.25, 129.71, 129.11, 128.49, 125.06, 124.27, 122.07, 121.21, 121.19, 110.54, 99.98, 48.95, 38.87, 26.64, 23.92, 20.75, 11.04, 11.01. MALDI-Tof/Tof-MS calcd for $C_{41}H_{44}N_3O_4^+$ 642.3326 $[M]^+$, found 642.1502 $[M]^+$.

General Synthetic Procedure of Compounds Cy7-2 and Cy7-3. Compound Cy7-Cl (100 mg, 0.156 mmol, 1 equiv) and corresponding 4-nitro aromatic compounds (0.47 mmol, 3 equiv) were dissolved in anhydrous *N*,*N*-dimethylformamide 10 mL), and the solution was stirred at room temperature for 24 h under argon protection. The solvent was then removed under reduced pressure. The crude product was purified by chromatography on silica (SiO_2; CH_2Cl_2/CH_3OH, 50:1, v/v) to afford target compounds (Figures S15−S20).

Cy7-2. A green solid with a metallic luster, 40% yield. ^{1}H NMR (400 MHz, MeOD) δ 8.37 (d, J = 9.4 Hz, 2H), 7.90 (d, J = 14.2 Hz, 2H), 7.41 (dd, J = 12.2, 8.3 Hz, 6H), 7.32−7.21 (m, 4H), 6.23 (d, J = 14.2 Hz, 2H), 4.19 (q, J = 7.2 Hz, 4H), 2.81 (t, J = 6.1 Hz, 4H), 2.16−2.03 (m, 2H), 1.48−1.31 (m, 18H). ^{13}C NMR (101 MHz, MeOD) δ 172.06, 163.99, 161.92, 141.62, 141.18, 141.11, 128.45, 126.32, 125.04, 122.08, 120.92, 120.91, 115.35, 115.34, 115.33, 110.52, 99.75, 99.74, 48.97, 38.82, 26.62, 23.79, 20.87, 11.01. MALDI-Tof/Tof-MS calcd for $C_{41}H_{44}N_3O_4^+$ 614.3383 $[M]^+$, found 614.3441 $[M]^+$.

Cy7-3. A green solid with a metallic luster, 59% yield. ^{1}H NMR (400 MHz, MeOD) δ 8.71 (d, J = 14.2 Hz, 2H), 8.19 (d, J = 9.1 Hz, 2H), 7.57−7.37 (m, 6H), 7.36−7.19 (m, 4H), 6.37 (d, J = 14.2 Hz, 2H), 4.22 (q, J = 7.2 Hz, 4H), 2.89−2.85 (m, 4H), 2.20−2.02 (m, 2H), 1.43 (dd, J = 23.8, 16.6 Hz, 18H). ^{13}C NMR (101 MHz, MeOD) δ 172.51, 146.70, 145.39, 141.65, 141.35, 133.25, 128.48, 125.86, 125.22, 124.18, 122.12, 110.67, 101.15, 49.16, 38.95, 26.56, 25.94, 20.62, 11.11. MALDI-Tof/Tof-MS calcd for $C_{41}H_{44}N_3O_4^+$ 630.3154 $[M]^+$, found 630.3177 $[M]^+$.

General Procedure for Nitroreductase Detection. All UV−vis, fluorescence, and quantum yield measurements were carried out in 0.05 M Tris buffer solution containing 1.5% DMSO, pH 7.4. In a 2 mL tube, Tris buffer (1 mL) and 1 mM Cy7-1 (20 μL) were mixed, and then NADH was added to obtain a final concentration of 500 μM. Nitroreductase was dissolved in Tris buffer, and an appropriate volume was added to the sample solution. The final solution volume was adjusted to 2 mL with Tris buffer. After rapid mixing of the solution, it was transferred to a 10 × 10 mm quartz cell and incubated at 37 °C for *in vitro* detection. Fluorescence spectra were recorded in the range from 750 to 850 nm with λ_{ex} = 730 nm from a xenon lamp, and absolute emission quantum yields were determined accordingly.

DFT Calculations. To delineate the nature of the ground and singlet excited states of compounds Cy7-1 and Cy7-NH_2, quantum chemical calculations were performed. All calculations, including the geometry optimization for Cy7-1−5 and Cy7-NH_2, were performed using the density functional theory (DFT), in conjunction with the B3LYP functional[12,13] and the 6-31G* basis set[14−18] for the ground-state and time-dependent DFT (TDDFT) replaced DFT for the singlet excited state, as implemented in the Gaussian 09 program package.[19]

Docking Calculations. The binding affinity calculations between probes Cy7-1−5 and nitroreductase were carried out on AutoDock software (4.2.6 version). The nitroreductase structure was obtained from PDB under code 4DN2, two chains and total 208 amino acid residues. The docking results and figures were obtained on AutoDock and LigPlot+.

HPLC for Nitroreductase Detection Assay. HPLC was performed on a Dionex P680A LPG-4 system with a Hypersil ODS2 column (250 × 4.6 mm, 5 μm, ThermoFisher). The conditions were as follows: volume ratio of methanol/H_2O = 100:0 (0 min) to 30:70 (20 min); flow rate 1 mL min^{-1}; detection under UV light at 254 nm.

Cell Culture. The A549 cell line was provided by the Institute of Biochemistry and Cell Biology, SIBS, CAS (China), which were grown in Dulbecco's modified Eagle's medium (DMEM) supplemented with 10% fetal bovine serum (FBS) and cultured at 37 °C under 5% CO_2 for normoxic condition (20% O_2). For hypoxia condition, A549 cells were cultured for 6 h at 37 °C under different O_2 concentration with 5% CO_2.

Confocal Fluorescence Imaging for Living Cells. A549 cells (5 × 10^8 /L) were plated on 14 mm glass coverslips and allowed to adhere for 12 h. The cells were washed with Tris buffer and then incubated with 5 μM Cy7-1 in DMSO/Tris buffer (1.5:98.5, v/v) for 10 min at 37 °C. Cells imaging was then carried out after washing cells with Tris buffer (2 mL × 3 times). Fluorescence imaging was performed with an Olympus FV1000 confocal fluorescence microscope with a 40 × oil immersion objective lens. The fluorescence signal of cells incubated with Cy7-1 was collected at 780 ± 30 nm, using semiconductor laser at 633 nm as excitation resource.

Cytotoxicity Assay. The *in vitro* cytotoxicity was measured using a standard methyl thiazolyl tetrazolium (MTT, Sigma-Aldrich) assay in A549 cell lines. Briefly, cells growing in log phase were seeded into 96-well cell-culture plate at 1 × 10^4/well. The probe Cy7-1 (100 μL/well) at concentrations of 2−25 μM was added to the wells of the treatment group, and 100 μL/well DMSO diluted in DMEM at final concentration of 0.5% to the negative control group, respectively. The cells were incubated for 6 and 12 h at 37 °C under 5% CO_2, respectively. The combined MTT/PBS solution was added to each well of the 96-well assay plate and incubated for an additional 4 h. An enzyme-linked immunosorbent assay (ELISA) reader (infinite M200, Tecan, Austria) was used to measure the OD570 (absorbance value) of each well referenced at 690 nm. The following formula was used to calculate the viability of cell growth: viability (%T) = ($A1$ − $A2$) × 100%, where $A1$ denotes absorbance value of treatment group, and $A2$ denotes absorbance value of control.

Murine Tumor Model. Animal procedures were in agreement with the guidelines of the Institutional Animal Care and Use Committee. About 10^6 A549 cells were grafted into a nude mouse. Tumors with diameters of around 7 and 12 mm were formed after 30 and 50 days, respectively.

Murine Acute Peritonitis Model. Animal procedures were in agreement with the guidelines of the Institutional Animal Care and Use Committee. According to a reported method,[20] 2% aqueous acetic acid solution (0.1 mL) was intraperitoneally injected into a nude mouse. After 2 h, the murine acute peritonitis model could be used.

Fluorescence *in Vivo* Imaging. Animal procedures were in agreement with the guidelines of the Institutional Animal Care and Use Committee. In this small animal *in vivo* fluorescence imaging system, adjustable 0−1.3 W power 730 nm continue wavelength laser (Connet Fiber Optics, China) was used as the excitation source, and the fluorescence signal was collected by Andor DU897 EMCCD with Semrock 800 ± 12 nm bandpass filter.

Positron Emission Tomography/Computed Tomography (PET/CT) *in Vivo*. Animal procedures were in agreement with the guidelines of the Institutional Animal Care and Use Committee. PET/CT imaging of the murine A549 tumor model was carried out with a Siemens Inveon PET/CT imaging system. The PET/CT imaging signal was collected from the A549 tumor-bearing mouse injected with 0.2 mL of 300 μCi ^{18}F-FMISO through intravenous injection after 90 min. The A549 tumor model was 12 mm in diameter.

DOI: 10.1021/jacs.5b04097
J. Am. Chem. Soc. 2015, 137, 6407−6416

Enzymatic Assays. Enzymatic assays were carried out by the SDS polyacrylamide gel electrophoresis (SDS-PAGE) method. Nitroreductase from *Escherichia coli* as a standard sample (ca. 24 kDa), proteome lysates from A549 tumors (diameters of 12 and 7 mm, test sample) and normal tissue beside the tumor (control sample) of the A549 tumor model mouse were prepared in RIPA (radio immunoprecipitation assay) lysis buffer (Beyotime Co.); a PageRuler Prestained Protein Ladder (10 to 170 kDa) was purchased from Thermo Scientific Co.

RESULTS AND DISCUSSION

Design and Synthesis of Cy7-1. Suitable fluorescent probes for *in vivo* NTR detection should meet certain requirements, such as an NIR optical window, enhanced fluorescence, fast and sensitive response, and good selectivity.[4a] It is necessary to take all of these characteristics into account to design a probe structure. Meanwhile, a fluorescent probe for NTR should consist of a detecting part and a fluorescence reporting part. In the present study, the detecting part and the fluorescence reporting unit are an aromatic nitro group and a cyanine structure, respectively. To optimize the probe structure, different connecting groups and different nitro positions were chosen to investigate the structure−function relationship. As shown in Scheme 1, fixing the *para*-nitro phenyl group and cyanine group and changing the connecting bond from −COO to O and S, the obtained probes Cy7-1, Cy7-2, and Cy7-3 have an insight into the influence of the connecting bond. Then, fixing the ester bond to connect the cyanine part and the aromatic group, nitro group was introduced from *para*-phenyl position to *ortho*-, and *meta*-phenyl position to obtain the probes Cy7-2 and Cy7-3 and explore the influence of aromatic nitro positions. Because the aromatic nitro group is strongly electron withdrawing, it is reasonable to assume that the fluorescence for these probes could be quenched.[11] After reacting with NTR, the nitro group can be reduced, and hence the intramolecular electron-transfer process is inhibited, which could correspond to the recovery of fluorescence emission of the cyanine.

Fluorescent probes Cy7-1, Cy7-4, and Cy7-5 were synthesized from another cyanine dye, Cy7-Cl, as the precursor (Scheme S1). Treatment of Cy7-Cl with sodium acetate in DMF gave a ketone structure, Cy7-OH, which could be protonated and converted into a more conjugated π-electron system.[21,22] Notably, Cy7-OH could only be conjugated with nitrobenzoyl chloride through an ester linkage under acidic condition, giving the target compounds Cy7-1, Cy7-4, and Cy7-5 (Schemes 2 and S2) in satisfactory yields of 48−77%. Under basic condition, Cy7-OH was deprotonated and reverted to the ketone structure. Probes Cy7-2 and Cy7-3 can be directly obtained from Cy7-Cl under basic conditions though a simple one-step reaction (Scheme S2). All intermediates and target compounds were characterized by ^{1}H NMR, ^{13}C NMR, or MALDI-Tof/Tof-MS spectrometry, giving satisfactory results.

Optical Properties of Cy7-1−5 to Nitroreductase. To understand the effect of the NTR-induced reduction reaction on the photophysical properties of Cy7-1−5, the absorption and fluorescence emission spectra of five probes were investigated. It is well-known that, with a small amount of DMSO or ethanol as co-solvent (ca. 1−10%), cyanine dyes can be easily dissolved in H_2O and buffer solution, such as phosphate or Tris buffer, as reported previously.[7,10,11,21,22] To avoid aggregation of Cy7-1−5 in the buffer system, the buffer system was identified as 0.05 M Tris with 1.5% DMSO as the co-solvent.

In this buffer system, all probes showed extended absorption regions from the visible to NIR, with their absorption maxima between 764 and 784 nm (Figure 1), and the absorption

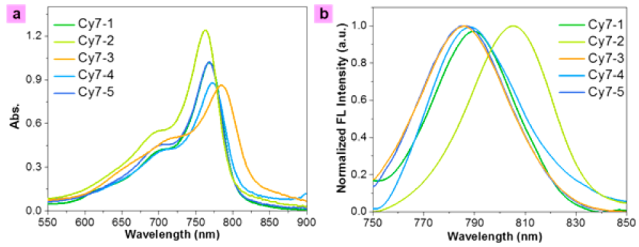

Figure 1. UV−vis absorption (a) and normalized fluorescence emission (b) spectra of Cy7-1−5 in 0.05 M Tris buffer with 1.5% DMSO as co-solvent, pH = 7.4.

maxima for these probes shifted ca. 20 nm. Under excitation at 730 nm, these probes displayed similar NIR emission bands, except Cy7-2 red shift ca. 20 nm. However, the fluorescence intensity of the probes were different, and the absolute quantum yields were measured as <0.1%, < 0.1%, 1.1%, < 0.1%, and 0.3%, respectively, for Cy7-1−5 in Tris buffer. These features indicated that the electron-withdrawing group induced electron-transfer process inhibited the fluorescence emission.

The response function of Cy7-1−5 to NTR was investigated by fluorescence emission spectroscopy, as depicted in Figures 2.

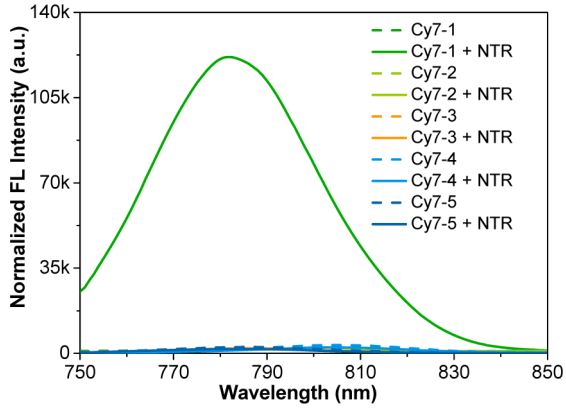

Figure 2. Normalized fluorescence spectra of Cy7-1−5 catalyzed by NTR (0.25 μg mL^{-1}) before (dash line) and after (solid line).

On adding 0.25 μg mL^{-1} NTR in the presence of NADH, no significant changes were observed for probes Cy7-2−5, but a significant enhancement of about 110-fold in fluorescence intensity was observed for Cy7-1. To identify the enhanced fluorescence came from the NTR reduced nitro to amino substance, the reduction product of Cy7-NH_2 was also synthesized for the investigation of its photophysical properties (Schemes 3 and S3 and Figure S22). Cy7-NH_2 displays similar NIR emission bands compared with Cy7-1, but the fluorescence intensity of Cy7-NH_2 is 2 orders of magnitude higher than that of Cy7-1, and the absolute quantum yield in Tris buffer was measured as 1.8%. According to the natural transition orbitals (NTOs) depicted in Figure S23, the lowest-energy absorption band resides on the cyanine π-conjugated moiety for both Cy7-1 and Cy7-NH_2. However, the results of DFT calculations on the singlet emitting states clearly indicated charge transfer from the cyanine π-conjugated moiety to the nitro aromatic moiety in the case of Cy7-1, and no charge

DOI: 10.1021/jacs.5b04097
J. Am. Chem. Soc. 2015, 137, 6407−6416

Scheme 3. Deduced Enzyme-Catalyzed Mechanism of Cy7-1 Activated with the Nitroreductase[a]

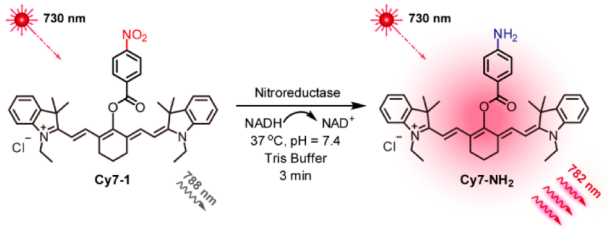

[a]NADH stands for β-nicotinamide adenine dinucleotide disodium salt hydrate.

transfer was monitored for Cy7-NH_2. This confirms that an intramolecular electro-withdrawing group induced electron-transfer process occurs in Cy7-1 but not in Cy7-NH_2, accounting for the fluorescence quenching in the former.

To demonstrate Cy7-NH_2 is the product of NTR-catalyzed Cy7-1, the MALD-Tof/Tof-MS spectrometric and HPLC analyses proved that the response of Cy7-1 to nitroreductase was related to the deduced enzyme-catalyzed mechanism (Scheme 3). The observation of a peak at m/z = 612.0567 in the MALD-Tof/Tof-MS spectrum, corresponding to Cy7-NH_2 ([M^+] 612.3590), confirmed that Cy7-1 had been reduced by NTR (Figure S24). Furthermore, as shown in Figure S25, standard samples of NADH, NTR, Cy7-1, and Cy7-NH_2 all showed distinctly different retention times, specifically 7.59, 10.46, 13.40, and 15.92 min, respectively. When Cy7-1 was mixed with NTR in the presence of NADH, after 10 min, besides a weak peak at 13.4 min corresponding to Cy7-1, a new peak at 15.92 min corresponding to Cy7-NH_2 was also observed in the HPLC trace (curve e), indicating that Cy7-1 had reacted with NTR to form Cy7-NH_2 in the presence of NADH. All of these data corroborated the deduced mechanism of the conversion of Cy7-1 into Cy7-NH_2 in the presence of NTR.

Docking Affinity of Cy7-1−5 to Nitroreductase. To get the deep understanding into the relationship between structure and NTR detection ability, docking calculations were carried out for Cy7-1−5 with nitroreductase. It should be noted that an effective NTR-catalyzed reaction involves a binding and catalysis processes and subsequently a departure process.[23] The formation of hydrogen bonding between substrate and NTR is critical for the catalytic step.

As shown in Figure 3a, the probe molecule tends to approach the hydrophobic interspace of NTR by the hydrophobic interaction and the aromatic rings $\pi-\pi$ interactions, then a transition state was formed utilizing hydrogen bonding between the NTR amino acid residues and nitro O atoms of Cy7-1. The probe Cy7-1 with a *para*-substituted nitro group formed eight hydrogen bonds with these amino acid residues Ser12, Ser14, Arg10, Arg11, and Arg 172 of NTR (Figure 3b).

In contrast, only one, two, two, and four hydrogen bonds were formed in Cy7-2−5 counterparts (Figure 3c−f). We visualized the interaction of Cy7-2−3 with NTR to study the effect of the linker −COO group in Cy7-1. As shown in Figure 3b−d, no hydrogen bond was observed between the O or S atoms of Cy7-2 or Cy7-3 and amino acid residues of NTR, while one hydrogen bond was formed in Cy7-1 with −COO

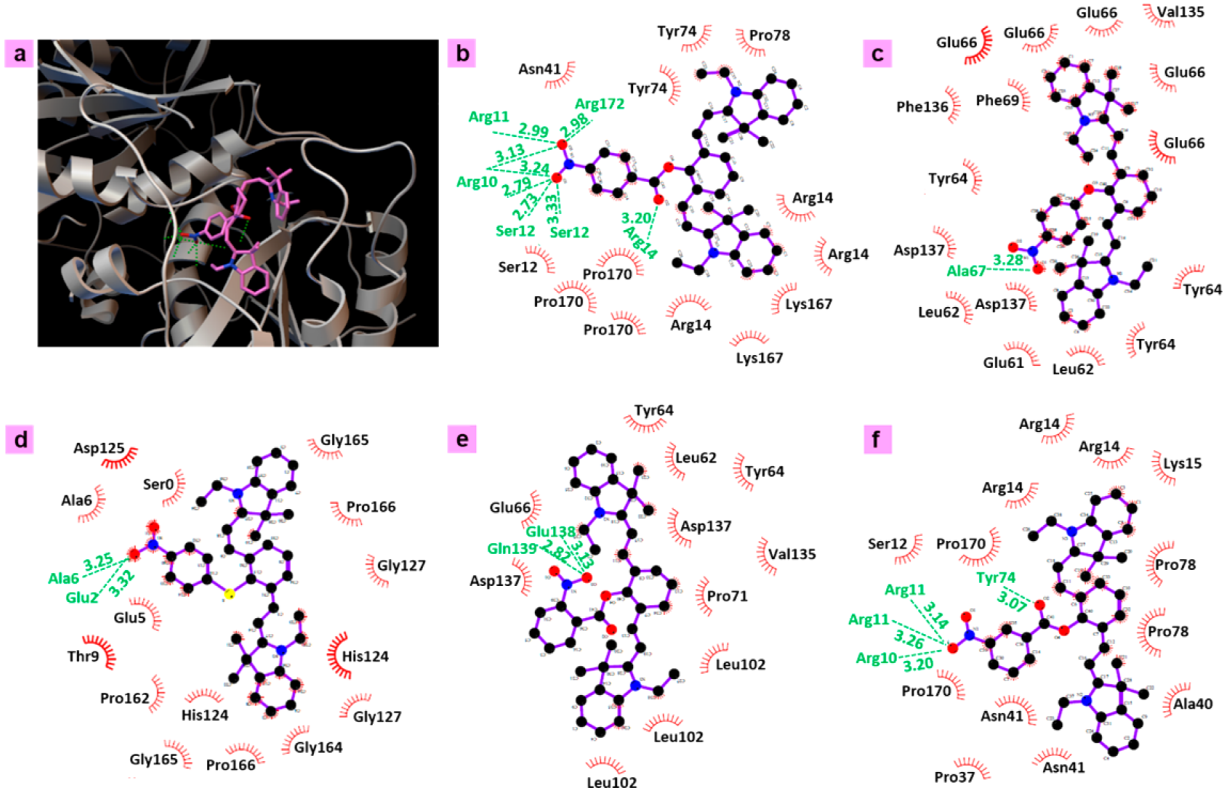

Figure 3. Calculated binding model of Cy7-1 (a, b), Cy7-2 (c), Cy7-3 (d), Cy7-4 (e), and Cy7-5 (f) with NTR. In (a), the C, N, and O atoms of Cy7-1 structure are shown in pink, blue, and red, respectively. In (b−f), the C, N, and O atoms of Cy7-1 to Cy7-5 structures are shown in black, blue, and red, respectively. Red curves are indicated the hydrophobic areas and the amino acid residues of the NTR. Hydrogen bonds are indicated with green dotted lines.

DOI: 10.1021/jacs.5b04097
J. Am. Chem. Soc. 2015, 137, 6407−6416

group as linker. Moreover, the spatial arrangement of Cy7-2 or Cy7-3 was not well matched with the hydrophilic interspace, thus only one or two hydrogen bonds were obtained between nitro group and amino acid residues. In stark contrast, there were seven hydrogen bonds between nitro O atoms of Cy7-1 and amino acid residues of NTR, indicating an optimal spatial structure match between Cy7-1 and NTR. This fact proved the linker between detection part and fluorescence reporting part is a key factor for the spatial structure match of the probe detecting part from the hydrophobic interspace to the hydrophilic interspace.

Additionally, fixing the ester connecting bond in the probe structure, we visualized the influence of nitro position by comparing the probes Cy7-4 and Cy7-5 contain *ortho*- and *meta*-nitro with Cy7-1 contain the *para*-nitro position. In Figure 3e,f, only two and three hydrogen bonds between nitro O atoms and amino acid residues for Cy7-4 and Cy7-5, with much less than seven hydrogen bonds in Cy7-1. We analyzed the chemical structures, it can be found that the distances between nitro O atoms and a fluorescence reporting cyanine part are 8.33 and 8.66 Å, 4.87 and 2.76 Å, and 6.2 and 7.66 Å for Cy7-1, Cy7-4, and Cy7-5, respectively (Figure S26). Therefore, the long distance between nitro O atoms and a fluorescence reporting part is beneficial for the probe approaching the amino acid residues of NTR hydrophilic part and forms strong hydrogen bonds with them. This fact could also be contributed to the enhancement in the spatial structure match and the NTR catalytic ability of Cy7-1.

Take all of these impact factors into consideration, the docking affinities are 8.1, 9.0. 8.4, 8.2, and 9.0 (kcal mol^{-1}) for Cy7-1 to Cy7-5, respectively. Note that the lower affinity value denotes the lower binding energy between probe and NTR, meaning that NTR can easily break away from reductive probe and then participate to the following catalytic process. Herein, the docking affinity values indicated that the chemical structure of Cy7-1 favors the departing process in the reaction, which also accelerate the catalytic cycles. All of these results consolidated the importance of the linker between detecting part and fluorescent reporting part and the nitro position and explained why Cy7-1 shows extremely high reactivity and sensitivity.

Optical Response of Cy7-1 to Nitroreductase. Since Cy7-1 has been demonstrated as a suitable NIR fluorescent probe for NTR detection, the kinetics of the interaction between Cy7-1 and NTR was further investigated by the fluorescence emission technique. As shown in Figure 4b, the fluorescence emission scan showed a significant enhancement within 1 min after the addition of NTR, suggesting an extremely fast response to the enzyme. Moreover, the time required to reach the maximum fluorescence intensity was progressively shortened with increasing NTR concentration (Figure 4c). An increased enzyme concentration enhances its catalytic ability and accelerates reduction of the nitro-containing probe to the fluorescent amine.[7] The same fluorescence enhancement could also be monitored using an EMCCD camera as the detector (Figure S27). Moreover, the maximum fluorescence intensity increased with the increase of NTR concentration, as shown in Figure 4d. This positive relationship indicated that the optical intensity could directly reflect the NTR concentration.

The reduction of Cy7-1 by NTR was optimized in terms of pH value and temperature (Figures S28 and S29). Under the optimized reaction condition (pH ≈ 7.4, T = 37 °C), the

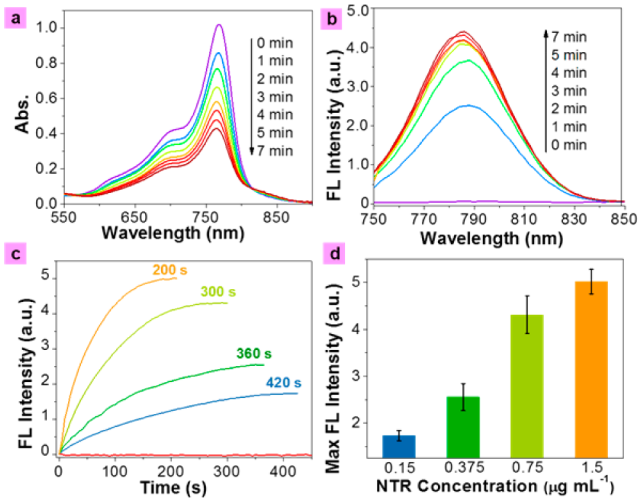

Figure 4. (a–b) Kinetic UV–vis absorption (a) and fluorescence (b) spectral scan of Cy7-1 (10 μM) reacted with NTR (0.25 μg mL^{-1}). (c) Time-dependent fluorescence emission intensity (λ_{ex} = 730 nm, λ_{em} = 782 nm) of Cy7-1 (10 μM) reacted with different NTR concentration of 0.15 μg mL^{-1} (blue), 0.375 μg mL^{-1} (green), 0.75 μg mL^{-1} (yellow), 1.5 μg mL^{-1} (orange), and without NTR (red). (d) The maximum emission intensity of Cy7-1 (10 μM) catalyzed by different NTR concentrations.

reduction of Cy7-1 with NTR led to increased fluorescence intensity, and good linearity was observed with the NTR concentration in the range of 0.15–0.45 μg mL^{-1} (Figure S30). The detection limit was determined as 1.14 ng mL^{-1} of NTR. Even under non-optimized conditions at pH 6.0 and room temperature (25 °C), the NTR could still catalyze the reduction of Cy7-1, and the emission intensity could be enhanced rapidly within 30 s and continue to enhance over 10 min (Figure S31). In addition, the kinetics of Cy7-1 cleavage by the enzyme was also investigated. Under the optimized condition, a Lineweaver–Burk double-reciprocal plot of 1/rate (V) versus 1/concentration was established as shown in Figure S32. The calculated values of apparent Michaelis–Menten constant K_m and maximum rate V_{max} were 190.3 μM and 0.086 μM s^{-1}, respectively.

To further study the reaction selectivity of Cy7-1, various potential interfering species were examined, such as salts (K^+, Na^+, Ca^{2+}), amino acids (tyrosine, glycine, glutamic acid, tryptophan, arginine), glucose, vitamin C, reactive oxygen species (H_2O_2, KO_2), lysozyme, and BSA. As shown in Figure 5, when these potential interfering species were added to Cy7-1 (10 μM) in the presence of 500 μM NADH, no significant fluorescence enhancement was observed. Strikingly, when 0.25 μg mL^{-1} NTR was added, significant fluorescence enhancement was observed as before. Furthermore, some interfering species in redox systems, such as electron transporters (cytochrome *b*5, cytochrome *c*) and oxidoreductases (leucine dehydrogenase, glutathione reductase, and formate dehydrogenase), were also investigated. As illustrated in Figure 6, these enzymes and electron transporters showed no reactivity toward Cy7-1 and did not interfere with the fluorescent response of Cy7-1 to NTR. Therefore, Cy7-1 shows excellent selectivity for NTR over other species.

An enzyme inhibition test also demonstrated that the fluorescence enhancement response of Cy7-1 to NTR arose from the enzyme-catalyzed reductase reaction. Dicoumarin is a common nitroreductase activity inhibitor.[24] When Cy7-1 was

DOI: 10.1021/jacs.5b04097
J. Am. Chem. Soc. 2015, 137, 6407–6416

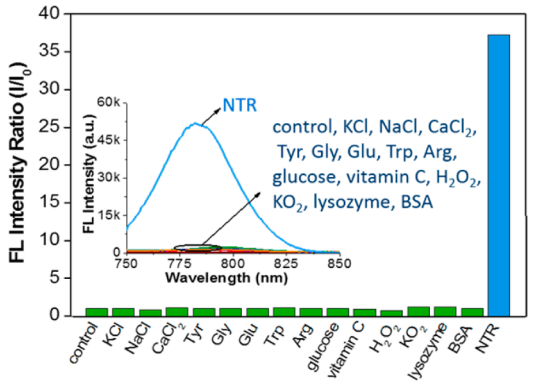

Figure 5. (a) Fluorescence responses at λ_{em} = 782 nm of Cy7-1 (10 μM) reacted with different kinds of species, blank (Cy7-1 + NADH), and with KCl (50 mM), NaCl (50 mM), $CaCl_2$ (50 mM), tyrosine (Tyr, 1 mM), glycine (Gly, 1 mM), glutamic acid (Glu, 1 mM), tryptophan (Trp, 1 mM), arginine (Arg, 1 mM), glucose (10 mM), vitamin C (1 mM), H_2O_2 (1 mM), KO_2 (1 mM), lysozyme (0.1 mg mL^{-1}), BSA (10 mg mL^{-1}), and nitroreductase (0.25 μg mL^{-1}). Inset is the fluorescence spectra of Cy7-1 reacted with different kinds of species. λ_{ex} = 730 nm.

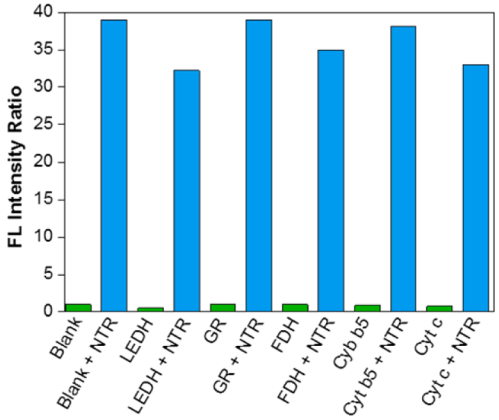

Figure 6. Fluorescence responses at 782 nm of Cy7-1 (10 μM) in DMSO-Tris buffer (pH 7.4, 1.5:98.5, v/v) to various redox species, in the presence of NADH (500 μM), at 37 °C. Bars represent the ratio of luminescence intensity at 782 nm. Green bars represent the cases in the absence of NTR. Blue bars represent the addition of NTR (0.25 μg mL^{-1}) to the above solution. LEDH: leucine dehydrogenase (10 μg mL^{-1}); GR: glutathione reductase (10 μg mL^{-1}); FDH: formate dehydrogenase (10 μg mL^{-1}); Cyt b5: cytochrome *b*5 (10 μg mL^{-1}); Cyt c: cytochrome *c* (10 μg mL^{-1}). λ_{ex} = 730 nm.

pre-treated with 0.1 mM dicoumarin and then mixed with NTR, the fluorescence intensity was much lower than that without dicoumarin (Figure S33). Moreover, increasing the concentration of dicoumarin led to a progressive decrease in the fluorescence intensity of a mixture of Cy7-1 and NTR, confirming that the NTR activity of Cy7-1 was inhibited by dicoumarin. Enzyme inhibition was also observed in another experiment, in which the fluorescence intensity of a mixture of Cy7-1 and NTR showed no obvious increase at 4 °C. These observations confirmed that the enhanced fluorescence response of Cy7-1 to NTR arises from an enzyme-promoted reductase reaction.

Photostability of the organic dye is important for NIR fluorescent detection *in vitro* and *in vivo*. After illumination at 730 nm by a 150 W xenon lamp for 30 min, the fluorescence intensity at λ_{em} = 788 nm of Cy7-1 buffer solution still remained at 90% (Figure S34), indicating good photostability of the dye under the detection condition.

Fluorescence Imaging of Nitroreductase in Hypoxic A549 Cells by Cy7-1. Before using Cy7-1 for its potential application as a bioprobe, it was necessary to check its biocompatibility. The cytotoxicity of Cy7-1 toward the A549 cell line (human alveolar basal epithelial cells) was determined by an MTT assay (Figure S35). In the presence of Cy7-1 at 2–25 μM, the cellular viabilities were estimated to be >70% after incubation for 6 or 12 h. The results indicated that Cy7-1 has low toxicity.

To assess the applicability of Cy7-1 for the intracellular NTR monitoring, confocal fluorescence microscopy was carried out on A549 cells, which are known to express NTR under hypoxic conditions.[7] A549 cells were grown under normoxic conditions (20% O_2) and different hypoxic conditions (10%, 5%, 3%, and 1% O_2) for 6 h, and then treated with 5 μM Cy7-1 for 10 min. As shown in Figure 7, A549 cells incubated under normoxic conditions showed a very weak NIR fluorescence signal. However, A549 cells showed increased fluorescence signals in the NIR region when cultured under decreased oxygen concentrations, indicating that these cells can express different NTR concentrations in different oxygen concentrations. The probe Cy7-1 could be catalytically reduced by the expressed NTR in cells cultured under different hypoxic conditions, giving rise to increased fluorescence intensities.

***In Vivo* Fluorescence Imaging of Nitroreductase in a Hypoxic A549 Tumor-Bearing Mouse Model by Cy7-1.** The suitability of Cy7-1 as a fluorescent probe for animal bioimaging *in vivo* was further investigated. After direct injection of Cy7-1 in Tris buffer into an A549 tumor of a living mouse, the emission was collected at 800 ± 12 nm by means of an EMCCD camera under CW excitation at 730 nm with a power density of 1 mW cm^{-2}.

To kinetically observe the change in the fluorescence intensity of Cy7-1 before and after injection into the mouse tumor, a tube loaded with Cy7-1 (20 μM) in Tris buffer was placed beside the mouse (Figure 8a). During long-term tracking, the Cy7-1 in the tube was essentially non-emissive. After injection of Cy7-1, the tumor region (d = 12 mm) showed a significant enhancement in fluorescence intensity within 2 s, and the highest fluorescence intensity at the injection site (ca. 8-fold higher) was attained within 3 min, as shown in Figure 8b,c and Videos S1 and S2. With extension of the tracking time, the increased fluorescence intensity gradually extended from the injection site and diffused to the whole tumor region. As verified previously, after injecting the Cy7-1 probe into the tumor, it was catalytically reduced to Cy7-NH_2 by the tumor-generated NTR, causing fluorescence of the whole tumor that lasted for more than 30 min.

Next, the inhibition *in vivo* was investigated. To this end, dicoumarin was again chosen as the inhibitor of NTR. When a mixture of Cy7-1 and dicoumarin was injected into the tumor region, the degree of enhancement (5-fold) of the fluorescence intensity was significantly lower than that (8-fold) without dicoumarin injection (Figure S36). Further inhibition of fluorescence enhancement was observed when dicoumarin was first injected into half of the tumor region and then Cy7-1 was injected 10 min later (Figure S37). Virtually no further fluorescence increase was observed in the tumor region injected with dicoumarin (ca. 0.3-fold). This inhibition further confirmed the catalytic reduction of Cy7-1 to emissive Cy7-NH_2 by the NTR in the tumor.

DOI: 10.1021/jacs.5b04097
J. Am. Chem. Soc. 2015, 137, 6407–6416

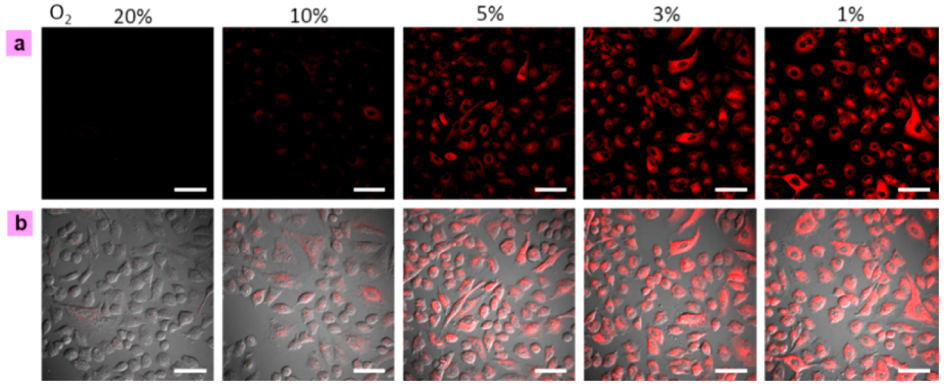

Figure 7. Confocal fluorescence microscopy imaging of A549 cells incubated with Cy7-1 (5 μM) under different oxygen concentration conditions. (a) The fluorescence imaging was collected at the near-IR channel (780 ± 30 nm, λ_{ex} = 633 nm semiconductor laser). (b) The merged fluorescence imaging and bright filed imaging. Scale bar = 60 μm.

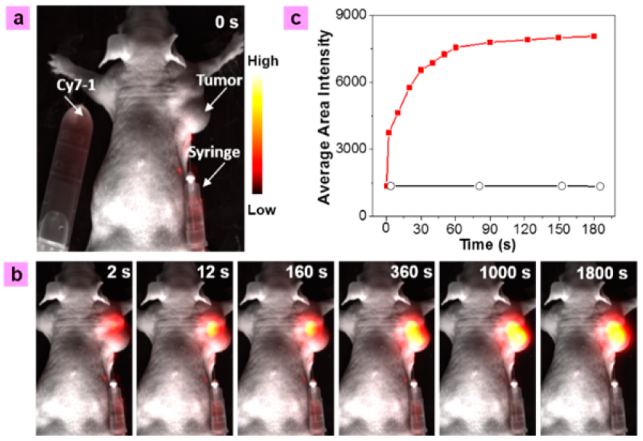

Figure 8. Time based *in vivo* fluorescence imaging of the A549 tumor mouse model before (a) and after (b) injecting Cy7-1 (20 μM, 100 μL) via intratumor injection. (c) The fluorescence intensity changing of Cy7-1 in tube (black) and mouse tumor region (red) at 0−180 s after injection. The fluorescence signal was collected at λ_{em} = 800 ± 12 nm under excitation with 730 nm CW laser (power density is 1 mW cm^{-2}).

In clinical studies, the PET technique has been commonly used to distinguish hypoxic from normoxic tumors, based on the fact that ^{18}F-FMISO can react with the tumor overexpressed NTR.[1a] In this work, such PET imaging confirmed that the A549 tumor in the murine model was a hypoxic tumor; as shown in Figure 9a, when ^{18}F-FMISO (300 μCi in 0.9% aqueous NaCl solution, 0.2 mL) was injected intravenously into the A549 tumor-bearing mouse after 90 min, a strong ^{18}F signal was observed in the tumor region. The conclusion of hypoxia was further confirmed by an enzyme assay (Figure S38). After completion of the PET imaging, the mouse was dissected. The A549 tumor tissue (test sample) and the normal tissue from beside the A549 tumor (control sample) were then subjected to electrophoresis for enzyme detection. As shown in Figure S39, the migration of NTR from the A549 tumor (2) was the same as that of the NTR marker (3) on the SDS−PAGE plate, and the enzyme molecular weight was ca. 24 kDa, comparable with that of the standard protein (4). In contrast, no enzyme or protein of the same molecular weight was obtained from the normal tissue (1).

Generally, with an increase in tumor size, the degree of hypoxia is intensified, and more NTR can be overexpressed.[1] The probe Cy7-1 was also investigated to monitor the degree of NTR overexpression in different sized A549 tumors (1, d = 7 mm, 2, d = 12 mm). As shown in Figures 9b,c, and S39, the fluorescence signal was enhanced by around 3- and 8-fold in the tumor region for mouse 1 (7 mm tumor) and mouse 2 (12 mm tumor), respectively. These distinct fluorescence enhancements reflect the different degrees of hypoxia in the different sized tumors; therefore, the probe Cy7-1 combined with fluorescent bioimaging provides a potential tool for *in vivo* monitoring of NTR overexpression and hypoxia level of the tumor. In Figure 9d, the same enzyme assay result was also obtained and verified for mouse 1 (left) optically imaged in Figure 9b.

Moreover, the probe Cy7-1 could be used to distinguish the hypoxic tumor from tissue showing inflammation tissue *in vivo*. Inflamed tissue can generate a certain amount of reactive oxygen.[25] However, when mixed with reactive oxygen, Cy7-1 in buffer solution cannot induce the fluorescence enhancement (Figure 5a, inset). Furthermore, a murine acute peritonitis model was chosen to investigate the *in vivo* interaction of Cy7-1 with reactive oxygen. The acute peritonitis mouse showed a serious edema and congestion in the enterocoelia (Figure S40) compared with a normal mouse; however, no significant fluorescence enhancement was observed in the whole enterocoelial region over a long period when Cy7-1 was injected intraperitoneally, in contrast to the 8-fold fluorescence enhancement in the tumor region (Figure 10). Therefore, Cy7-1 represents a novel NIR probe and can distinguish a hypoxic tumor from inflamed tissue by *in vivo* bioimaging. In addition, using Cy7-1 as a probe, the bioimaging penetration depth was investigated with artificial tissue.[26] With the laser excitation power density fixed at 1 mW cm^{-2}, the fluorescence intensity decreased with increasing thicknesses of artificial tissue (Figure S41). When the excitation power intensity was increased and the artificial tissue thickness was set at 6 mm, the signal could be monitored, and the signal-to-noise ratio was increased to around 3 (Figure S42). This demonstrated that Cy7-1 could be applied as an excellent bioimaging probe with good light penetration depth and low NIR excitation power density.

■ CONCLUSIONS

In summary, we have enriched the principle for designing a probe for nitroreductase detection. Experimental and docking theoretical calculation studies demonstrated the critical factors for design a suitable probe, not only involving the electro-

DOI: 10.1021/jacs.5b04097
J. Am. Chem. Soc. 2015, 137, 6407−6416

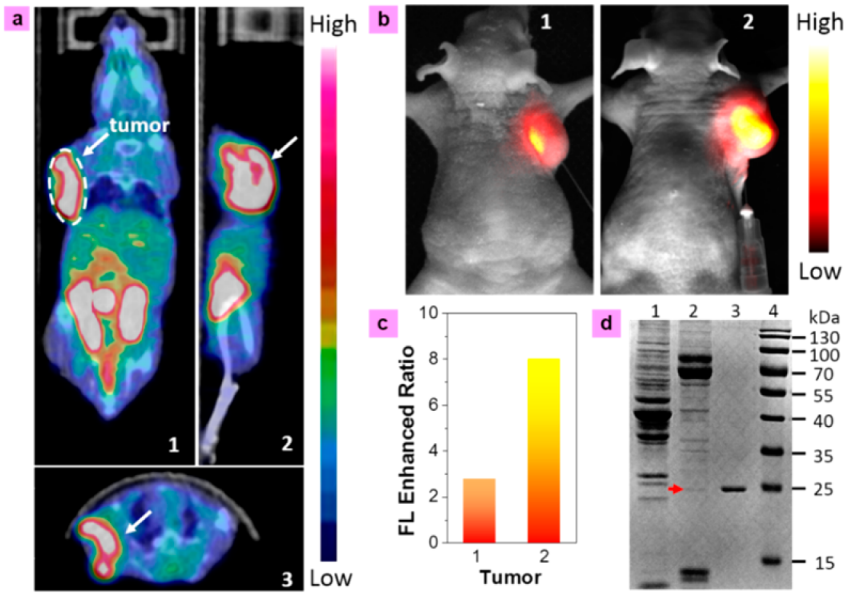

Figure 9. (a) The PET/CT imaging of A549 tumor−bearing mouse (tumor, d = 12 mm) through intravenous injection of the ^{18}F-FMISO (300 μCi in 0.9% NaCl aq. solution, 0.2 mL) after 90 min, (1) coronal plane, (2) sagittal plane, and (3) transverse plane. (b) Fluorescent *in vivo* imaging of the A549 tumor−bearing mouse models (left tumor 1 of 7 mm, right tumor 2 of 12 mm) through intratumor injection of 20 μM Cy7-1 in 0.05 M Tris buffer solution (100 μL) after 5 min the fluorescence signal was collected at 800 ± 12 nm under 730 nm irradiation with a power density of 1 mW cm^{-2}. (c) Fluorescence-enhanced ratio in tumor region of A549 tumor-bearing mice shown in (b). (d) The enzymatic assays results of the left mouse 1 in (b), (1) the normal tissue beside the A549 tumor sample, (2) A549 tumor tissue sample, (3) NTR marker, and (4) the standard protein molecular weight.

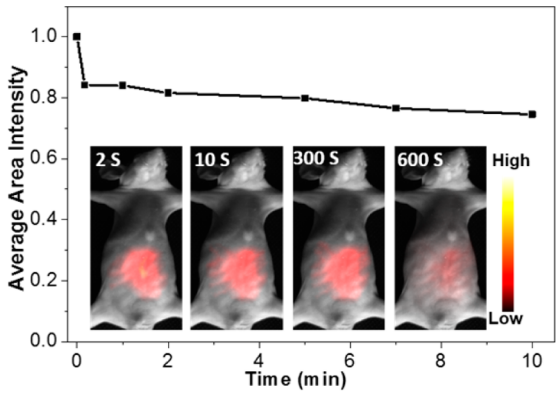

Figure 10. Fluorescence intensity change of Cy7-1 (20 μM, 200 μL) injected into the acute peritonitis model mouse. Inset, time-based *in vivo* fluorescence imaging of Cy7-1 injected into the model mouse via intraperitoneal injection. The fluorescence signals were collected at λ_{em} = 800 ± 12 nm under exciation with 730 nm CW laser (power density is 1 mW cm^{-2}).

withdrawing group induced charge transfer process but also the hydrogen bind formation between NTR and substance and the structural and spatial match-mismatch of these two. Those factors have been significantly influenced by the linker between probe detecting part and fluorescent reporting part and the position of nitro substituent in substrate. On the basis of the principle, among designed five probes (Cy7-1−5), only the *para*-nitro aromatic group decorated cyanine probe through ester bond linked probe (Cy7-1) displayed a fast response (<1 min), high sensitivity, and excellent selectivity, with a fluorescence turn-on (ca. 110-fold) response to NTR. Kinetic optical studies and other experiments support the proposed NTR catalytic reduction mechanism. The nitro group of Cy7-1 is reduced by NTR to generate Cy7-NH_2, which inhibits an electro-withdrawing group induced electron-transfer process and causes a fluorescence enhancement. Confocal fluorescence imaging of hypoxic A549 cells with overexpressed NTR demonstrates the NTR detection ability of Cy7-1 at the cellular level. More importantly, the hypoxic A549 tumor fluoresces within 2 s of injecting Cy7-1, and the effect lasted for a long time (at least 30 min). Cy7-1 can not only be used to discern the degrees of hypoxia of different sized tumors but can also distinguish a hypoxic tumor from inflamed tissue *in vivo*, further highlighting the potential diagnostic application of Cy7-1. This hypoxic tumor optical imaging method is convenient, simple to operate, and inexpensive. Our successful NIR fluorescent turn-on system provides a new design strategy for further novel probes for highly sensitive *in vivo* nitroreductase imaging studies.

■ ASSOCIATED CONTENT

Supporting Information

Photophysical and computational data, some fluorescence imaging figures and *in vivo* NTR detection movies Video S1 (30 s, fast response), Video S2 (long-term tracking). The Supporting Information is available free of charge on the ACS Publications website at DOI: 10.1021/jacs.5b04097.

■ AUTHOR INFORMATION

Corresponding Authors

*fyli@fudan.edu.cn
*fengweifd@fudan.edu.cn

Notes

The authors declare no competing financial interest.

■ ACKNOWLEDGMENTS

This study was supported by the State Key Basic Research Program of China (2015CB931800 and 2013CB733700), the

DOI: 10.1021/jacs.5b04097
J. Am. Chem. Soc. 2015, 137, 6407−6416

National Science Foundation of China (21231004 and 21375024) and the China Postdoctoral Science Foundation (2013M541457) for financial support.

REFERENCES

(1) (a) Padhani, A. R.; Krohn, K. A.; Lewis, J. S.; Alber, M. *Eur. Radiol.* **2007**, *17*, 861. (b) Wilson, W. R.; Hay, M. P. *Nat. Rev. Cancer* **2011**, *11*, 393. (c) Brown, J. M.; William, W. R. *Nat. Rev. Cancer* **2004**, *4*, 437. (d) Chen, Y.; Hu, L. *Med. Res. Rev.* **2009**, *29*, 29.

(2) Okuda, K.; Okabe, Y.; Kadonosono, T.; Ueno, T.; Youssif, B. G. M.; Kizaka−Kondoh, S.; Nagasawa, H. *Bioconjugate Chem.* **2012**, *23*, 324.

(3) (a) Xu, G.; Mcleod, H. L. *Clin. Cancer Res.* **2001**, *7*, 3314. (b) Parkinson, G. N.; Skelly, J. V.; Neidle, S. *J. Med. Chem.* **2000**, *43*, 3624.

(4) (a) Yang, Y.; Zhao, Q.; Feng, W.; Li, F. *Chem. Rev.* **2013**, *113*, 192. (b) Shi, Y.; Zhang, S.; Zhang, X. *Analyst* **2013**, *138*, 1952. (c) Huang, H.; Wang, K.; Huang, S.; Lin, H.; Lin, C. *Biosens. Bioelectron.* **2011**, *26*, 3511.

(5) (a) Cui, L.; Zhong, Y.; Zhu, W.; Xu, Y.; Du, Q.; Wang, X.; Qian, X.; Xiao, Y. *Org. Lett.* **2011**, *13*, 928. (b) Guo, T.; Cui, L.; Shen, J.; Zhu, W.; Xu, Y.; Qian, X. *Chem. Commun.* **2013**, *49*, 10820. (c) Yuan, J.; Xu, Y.; Zhou, N.; Wang, R.; Qian, X.; Xu, Y. *RSC Adv.* **2014**, *4*, 56207.

(6) (a) Li, Z.; Li, X.; Gao, X.; Zhang, Y.; Shi, W.; Ma, H. *Anal. Chem.* **2013**, *85*, 3926. (b) Li, Z.; He, X.; Wang, Z.; Yang, R.; Shi, W.; Ma, H. *Biosens. Bioelectron.* **2015**, *63*, 112.

(7) Xu, J.; Sun, S.; Li, Q.; Yue, Y.; Li, Y.; Shao, S. *Analyst* **2015**, *140*, 574.

(8) (a) Wang, X.; Stolwijk, J. A.; Lang, T.; Sperber, M.; Meier, R. J.; Wegener, J.; Wolfbeis, O. S. *J. Am. Chem. Soc.* **2012**, *134*, 17011. (b) Kiyose, K.; Hanaoka, K.; Oushiki, D.; Nakamura, T.; Kajimura, M.; Suematsu, M.; Nishimatsu, H.; Yamane, T.; Terai, T.; Hirata, Y.; Nagano, T. *J. Am. Chem. Soc.* **2010**, *132*, 15846. (c) Takahashi, S.; Piao, W.; Matsumura, Y.; Komatsu, T.; Ueno, T.; Terai, T.; Kamachi, T.; Kohno, M.; Nagano, T.; Hanaoka, K. *J. Am. Chem. Soc.* **2012**, *134*, 19588. (d) Achatz, D. E.; Meier, R. J.; Fischer, L. H.; Wolfbeis, O. S. *Angew. Chem.* **2011**, *123*, 274. (e) Yoshihara, T.; Yamaguchi, Y.; Hosaka, M.; Takeuchi, T.; Tobita, S. *Angew. Chem., Int. Ed.* **2012**, *51*, 4148. (f) Zhang, S.; Hosaka, M.; Yoshihara, T.; Negishi, K.; Iida, Y.; Tobita, S.; Takeuchi, T. *Cancer Res.* **2010**, *70*, 4490.

(9) (a) Wu, X.; Sun, X.; Guo, Z.; Tang, J.; Shen, Y.; James, T. D.; Tian, He.; Zhu, W. *J. Am. Chem. Soc.* **2014**, *136*, 3579. (b) Wu, X.; Chang, S.; Sun, X.; Guo, Z.; Li, Y.; Tang, J.; Shen, Y.; Shi, J.; Tian, H.; Zhu, W. *Chem. Sci.* **2013**, *4*, 1221. (c) Qu, Y.; Hua, J.; Tian, H. *Org. Lett.* **2010**, *12*, 3320. (d) Wang, J.; Song, F.; Wang, J.; Peng, X. *Analyst* **2013**, *138*, 3667. (e) Zhang, C.; Zhao, J.; Wu, S.; Wang, Z.; Wu, W.; Ma, J.; Guo, S.; Huang, L. *J. Am. Chem. Soc.* **2013**, *135*, 10566. (f) Niu, L.; Guan, Y.; Chen, Y.; Wu, L.; Tung, C.; Yang, Q. *Chem. Commun.* **2013**, *49*, 1294. (g) Niu, L.; Guan, Y.; Chen, Y.; Wu, L.; Tung, C.; Yang, Q. *J. Am. Chem. Soc.* **2012**, *134*, 18928.

(10) Xu, K.; Wang, F.; Pan, X.; Liu, R.; Ma, J.; Kong, F.; Tang, B. *Chem. Commun.* **2013**, *49*, 2554.

(11) Wang, R.; Yu, F.; Chen, L.; Chen, H.; Wang, L.; Zhang, W. *Chem. Commun.* **2012**, *48*, 11757.

(12) Axel, D. B. *J. Chem. Phys.* **1993**, *98*, 5648.

(13) Lee, C.; Yang, W.; Parr, R. G. *Phys. Rev. B* **1988**, *37*, 785.

(14) Clark, T.; Chandrasekhar, J.; Spitznagel, G. W.; Schleyer, P. V. R. *J. Comput. Chem.* **1983**, *4*, 294.

(15) Francl, M. M.; Pietro, W. J.; Hehre, W. J.; Binkley, J. S.; Gordon, M. S.; DeFrees, D. J.; Pople, J. A. *J. Chem. Phys.* **1982**, *77*, 3654.

(16) Gill, P. M. W.; Johnson, B. G.; Pople, J. A.; Frisch, M. J. *Chem. Phys. Lett.* **1992**, *197*, 499.

(17) Hariharan, P. C.; Pople, J. A. *Theor. Chim. Acta* **1973**, *28*, 213.

(18) Krishnan, R.; Binkley, J. S.; Seeger, R.; Pople, J. A. *J. Chem. Phys.* **1980**, *72*, 650.

(19) Frisch, M. J.; Trucks, G. W.; Schlegel, H. B.; Scuseria, G. E.; Robb, M. A.; Cheeseman, J. R.; Scalmani, G.; Barone, V.; Mennucci, B.; Petersson, G. A.; Nakatsuji, H.; Caricato, M.; Li, X.; Hratchian, H. P.; Izmaylov, A. F.; Bloino, J.; Zheng, G.; Sonnenberg, J. L.; Hada, M.; Ehara, M.; Toyota, K.; Fukuda, R.; Hasegawa, J.; Ishida, M.; Nakajima, T.; Honda, Y.; Kitao, O.; Nakai, H.; Vreven, T.; Montgomery, J. A., Jr.; Peralta, J. E.; Ogliaro, F.; Bearpark, M.; Heyd, J. J.; Brothers, E.; Kudin, K. N.; Staroverov, V. N.; Kobayashi, R.; Normand, J.; Raghavachari, K.; Rendell, A.; Burant, J. C.; Iyengar, S. S.; Tomasi, J.; Cossi, M.; Rega, N.; Millam, J. M.; Klene, M.; Knox, J. E.; Cross, J. B.; Bakken, V.; Adamo, C.; Jaramillo, J.; Gomperts, R.; Stratmann, R. E.; Yazyev, O.; Austin, A. J.; Cammi, R.; Pomelli, C.; Ochterski, J. W.; Martin, R. L.; Morokuma, K.; Zakrzewski, V. G.; Voth, G. A.; Salvador, P.; Dannenberg, J. J.; Dapprich, S.; Daniels, A. D.; Farkas, Ö.; Foresman, J. B.; Ortiz, J. V.; Cioslowski, J.; Fox, D. J. *Gaussian 09*, Revision A.1; Gaussian, Inc.: Wallingford, CT, 2009.

(20) Clementi, G.; Caruso, A.; Maria, V.; Cutuli, C.; Prato, A.; Mangano, N. G.; Amico−Roxas, M. *Life Sci.* **1999**, *65*, 203.

(21) Guo, Z.; Nam, S. W.; Park, S.; Yoon, J. *Chem. Sci.* **2012**, *3*, 2760.

(22) Wang, X.; Sun, J.; Zhang, W.; Ma, X.; Lv, J.; Tang, B. *Chem. Sci.* **2013**, *4*, 2551.

(23) Haynes, C. A.; Koder, R. L.; Miller, A. F.; Rodgers, D. W. *J. Biol. Chem.* **2002**, *277*, 11513.

(24) Koder, R. L.; Miller, A. F. *Biochim. Biophys. Acta* **1998**, *1387*, 395.

(25) Jaeschke, H. *J. Gastroen. Hepatol.* **2011**, *26*, 173.

(26) Grand, A. M. D.; Lomnes, S. J.; Ohnishi, S.; Morgan, T. G.; Gogbashian, A.; Laurence, R. G.; Frangioni, J. V. *J. Biomed. Opt.* **2006**, *11*, 014007.

DOI: 10.1021/jacs.5b04097
J. Am. Chem. Soc. 2015, 137, 6407−6416